# Ultrafast Response p-Si/n-ZnO Heterojunction Ultraviolet Detector Based on Pyro-Phototronic Effect

*Zhaona Wang, Ruomeng Yu, Xingfu Wang, Wenzhuo Wu, and Zhong Lin Wang**

Room temperature ultraviolet (UV) detection has attracted tremendous attentions for defense technology, aerospace technique, flame warning, and chemical/biological analysis.[1] Considering the wide bandgap (3.3 eV), high exciton binding energy (60 meV), and property of environmental friendly,[2–4] ZnO has become one of the ideal materials for room temperature UV sensing applications.[5–9] Various ZnO-based UV photodetectors (PDs) have been reported with high photoresponsivity and/or detectivity, however, the typical response and recovery time of these PDs are ranging from several tens of microseconds to few hours in most cases.[10–16] Moreover, the response/recovery time is highly dependent on the ambient gas conditions due to the trapping mechanism controlled by the process of oxygen adsorption to and desorption from the ZnO nanowires (NWs) surface.[6,14,17] Normally, even longer response time is expected for ZnO-based UV sensors operating in vacuum or oxygen-deficient environments.[6,17] This issue has long been an obstacle to improving the ZnO-based UV sensing performances and prevented them from practical applications.[18] Therefore, it is necessary and essential to develop new working mechanism for ultrafast response/recovery UV sensing devices based on ZnO micro/nanostructures.

For wurtzite-structured ZnO NWs, pyroelectric polarizations are induced by changing temperatures across the material due to the non-central-symmetric crystal structures.[19,20] Upon light illuminations, a rapid increase in temperature is naturally induced within ZnO NWs, leading to a distribution of pyroelectric potentials along the crystal with pyro-polarization-charges presenting at both ends of the NW.[19,21] By forming a p-n heterojunction between n-ZnO and p-type semiconductors, these light-induced pyroelectric charges can effectively and fastly tune/control the charge transport across the interface/junction and modulate the optoelectronic processes of local carriers, such as generation, separation, diffusion, and recombination. This is the pyro-phototronic effect,[22] a three-way coupling effect among pyroelectric effect, photonic excitations, and semiconductor properties, which provides an alternative to achieve ultrafast photosensing performances through optoelectronic processes.

In this work, an UV nanosensor based on p-Si/n-ZnO NWs heterojunctions is carefully studied and systematically characterized. The light-self-induced pyro-phototronic effect in ZnO is utilized to modulate the optoelectronic processes and thus enhance the performances of UV sensing in different ambient gas conditions (i.e., air and vacuum). The response time of these p-Si/n-ZnO UV PDs is improved from 59 to 19 μs at the rising edge, and 40 to 22 μs at the falling edge by the pyro-phototronic effect in air. The photoresponsivity $R$ is enhanced by up to 599% regarding to the relative changes of transient current in air. Similar UV sensing performances are derived in vacuum as well. This work provides a novel design mechanism to achieve ultrafast UV sensing performances at room temperature in air/vacuum. The demonstrated ultrafast UV sensing devices may find broad applications in photosensing, optothermal detections, health monitoring, and other optoelectronic processes.

The structure of p-Si/n-ZnO PD is schematically illustrated in **Figure 1**a. A p-type Si wafer is washed by deionized (DI) water, and alcohol and dried at room temperature, followed by sputtering a thin layer of ZnO (100 nm) as seed layer for low temperature hydrothermal growth of ZnO NWs array to form p-Si/n-ZnO heterojunctions.[23,24] Side-view and top-view scanning electron microscopy (SEM) images presented in Figure 1b1,b2 indicate ZnO NWs array with diameters of 50–70 nm and lengths of 500 nm. Indium-tin oxide (ITO) is deposited on ZnO NWs as the transparent top-electrode, and copper is sputtered on the p-type Si as bottom-electrode. Detailed fabrication processes and measurement setup are found in the Experimental Section.

Relevant energy levels of the materials used to fabricate the p-Si/n-ZnO UV PDs are depicted in Figure 1c. The valence band (VB) and conduction band (CB) of the silicon and ZnO are –5.22 and –4.05 eV,[25] –7.71 and –4.35 eV,[26] versus vacuum, respectively. Upon 325 nm UV illumination, photo-induced free carriers are generated in the ZnO layer according to the transmission spectra of ZnO NWs array as shown in Figure S1 of the Supporting Information. The energy band alignment of the device ensures that electrons inject from the photosensitive layer (ZnO) and is collected at ITO electrode, while the valence band holes reaching the Cu electrode through the silicon. $I$–$V$ characteristics of the p-Si/n-ZnO PDs under 325 nm illumination are measured and plotted in Figure 1d, showing good UV response of the reversely biased device.[27] The reversal saturation currents increase monotonously as increasing the power density under each bias voltage. At –2.0 V bias voltage, the output current increases from 3.0 (dark) to 95.8 μA ($3.7 \times 10^{-3}$ W cm$^{-2}$) as shown in Figure S2 of the Supporting Information.

Dr. Z. Wang
Department of Physics
Applied Optics Beijing Area Major Laboratory
Beijing Normal University
Beijing 100875, China
R. Yu, X. Wang, Dr. W. Wu, Prof. Z. L. Wang
School of Materials Science and Engineering
Georgia Institute of Technology
Atlanta, GA 30332-0245, USA
E-mail: zhong.wang@mse.gatech.edu
Prof. Z. L. Wang
Beijing Institute of Nanoenergy and Nanosystems
Chinese Academy of Sciences
Beijing 100083, China

**DOI: 10.1002/adma.201600884**

ADVANCED MATERIALS
www.advmat.de

www.MaterialsViews.com

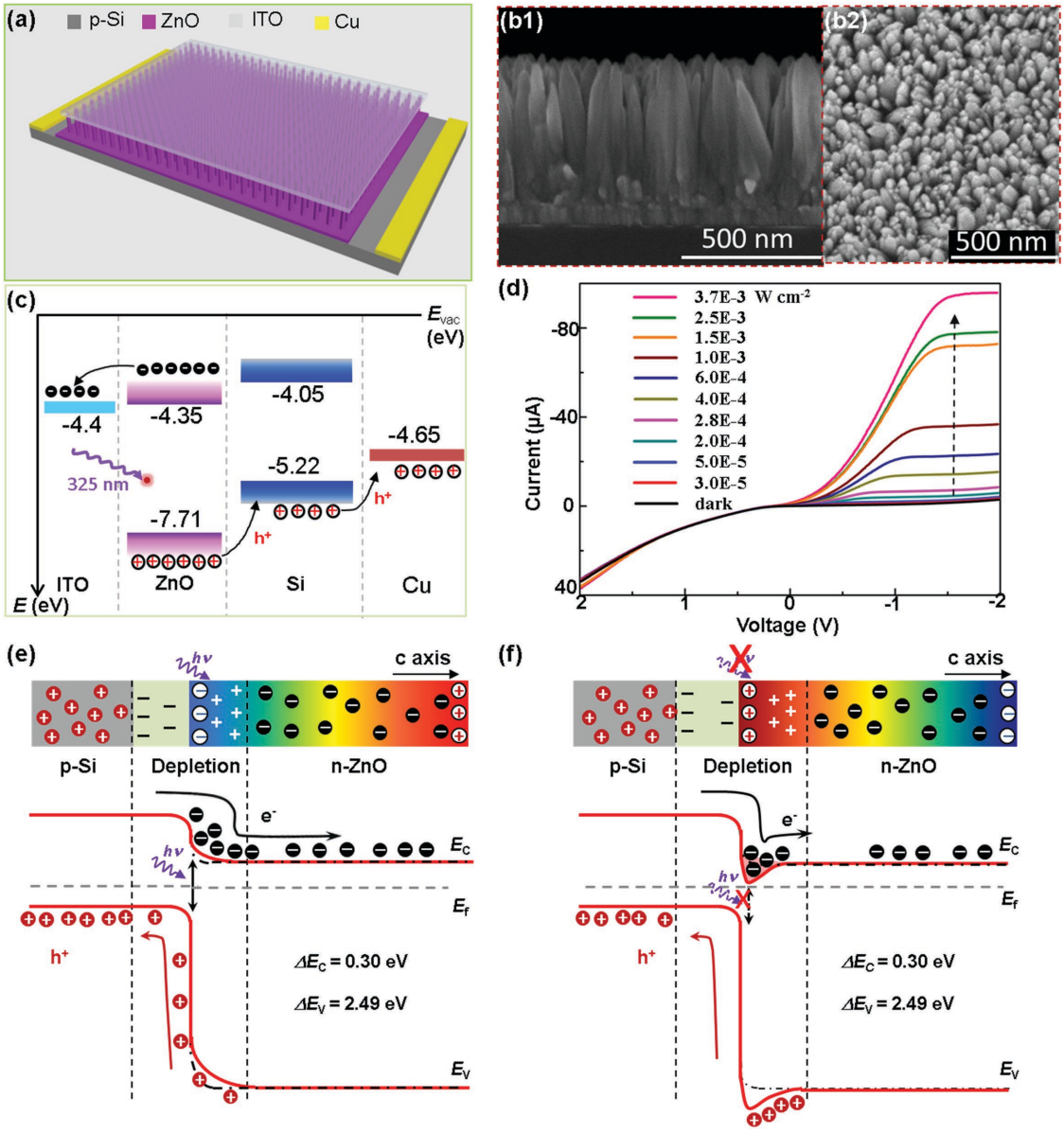


**Figure 1.** Structure, characterization, and working mechanism of pyro-phototronic effect based UV sensors. a) Schematic demonstration of the structure of pyro-phototronic effect based UV sensors. b1,b2) Scanning electron microscopy (SEM) images of ZnO nanowires (NWs) array: (b1) side view and (b2) top view. c) Energy band diagram of pyro-phototronic effect based UV sensors. Energies are expressed in electron volts, using the electron energy in vacuum as a reference. d) *I–V* characteristics of the pyro-phototronic effect based PD under dark and 325 nm laser illumination with different power densities. The arrow points out the increasing direction of laser power density. e,f) Schematic band diagrams of p-Si/n-ZnO heterojunction (e) as turning on and (f) turning off light to illustrate the working mechanism of pyro-phototronic effect based PDs.

The working mechanism of pyro-phototronic effect based PDs is schematically illustrated in Figure 1e,f. Upon UV illumination, a light-self-induced transient temperature increase appears within ZnO NWs during a rapid process of nanosecond scale,[22] which leads to negative pyro-polarizations distributed at local interface of pn heterojunction as shown in Figure 1e. Both the conduction and valence band of ZnO at the interface of pn junction increase as a result based on Anderson's model (Figure 1e).[25,28] Therefore, the charge carriers' transport across the heterojunction is significantly enhanced during this process and hence a transient high output current is observed from the measurements (**Figure 2**a). The temperature variation vanishes rapidly,[22] and the photocurrent gradually stabilizes at some certain value due to the relatively slow photoexcitation process. At the moment of turning off the UV illumination, a similar rapid process of transient temperature decrease happens within ZnO NWs, leading to the presence of positive pyro-polarizations at the local pn junction. The conduction and valence band of ZnO decrease and form a "carrier trap" effect due to positive pyro-polarizations as shown in Figure 1f.[25,28] Such "trap" greatly hinders the carriers' transport across the pn junction and the dark current is greatly reduced. Moreover, since the pyroelectric



*Adv. Mater.* **2016**,
DOI: 10.1002/adma.201600884

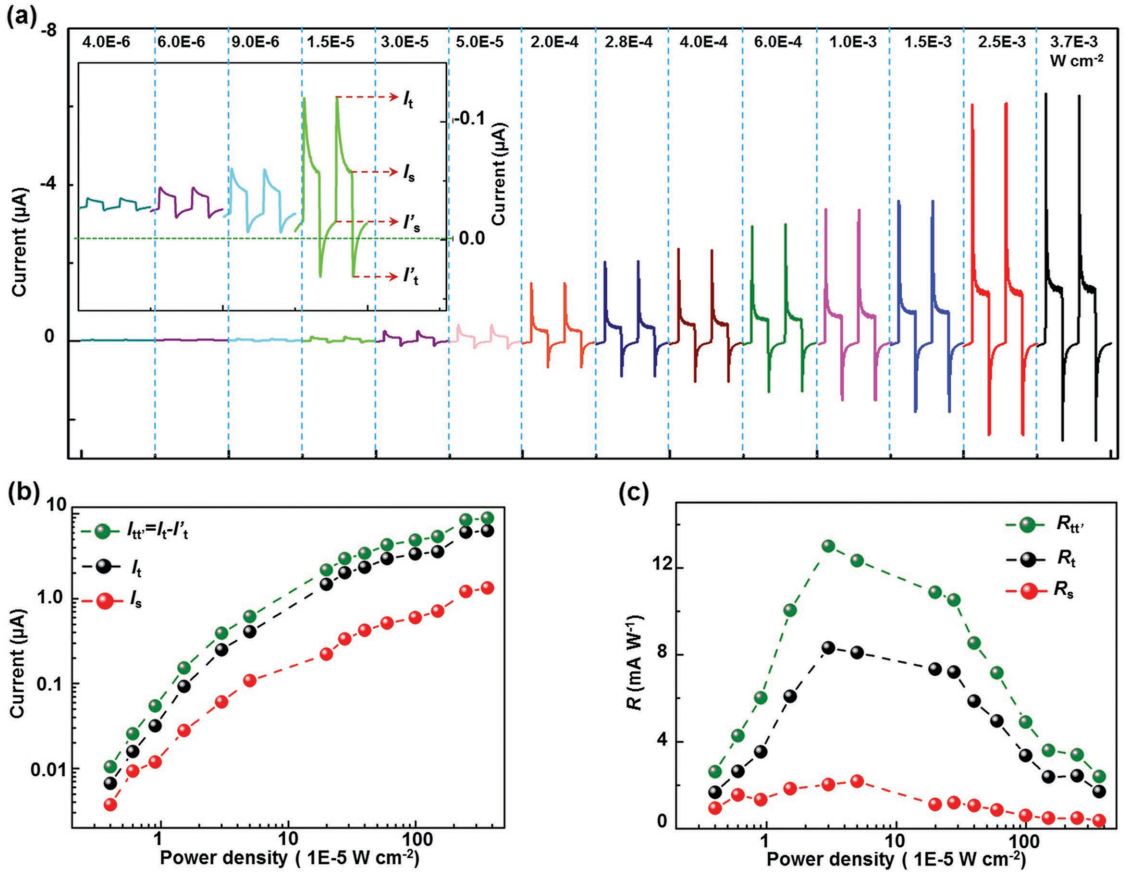


**Figure 2.** Pyro-phototronic effect enhanced performances of p-Si/n-ZnO UV sensors. a) *I–t* characteristics of pyro-phototronic effect based PD under 325 nm illuminations with different power densities from $4.0 \times 10^{-6}$ to $3.7 \times 10^{-3}$ W cm$^{-2}$, the inset is the enlarged *I–t* curves under the corresponding illumination conditions. b) The absolute transient ($I_t$, in black), absolute stable ($I_s$, in red) and relative transient ($I_{tt'}$, in olive) currents, c) and the corresponding photoresponsivity *R* change with the power densities, showing the enhancements by the pyro-phototronic effect. Data reported in (b) and (c) were calculated from *I–t* curves in (a).

potential induced from this rapid process is opposing the direction of bias voltage, reversed currents are observed transiently at low bias voltage cases (Figure 2a). This is the fundamental working mechanism of pyro-phototronic effect enhanced performances of p-Si/n-ZnO UV PDs. The response time and photoresponsivity of these sensors are significantly improved by utilizing the pyro-phototronic effect as elaborated below in detail.

The output current response of the pn heterojunction PDs to UV illumination are systematically investigated and summarized in Figure 2a by varying the power densities from $4.0 \times 10^{-6}$ to $3.7 \times 10^{-3}$ W cm$^{-2}$ and utilizing an optical chopper with 20 Hz in frequency when top ITO electrode is biased at 0.04 V. Under each power density, typical four-stage current responses to UV illumination are derived in each light pulse cycle. At the first stage, a sharp peak is induced by the pyro-phototronic effect upon 325 nm UV illuminations due to an instantaneous temperature increase within ZnO. The corresponding maximal output current is labeled as $I_t$, where subscripts "t" indicate the transient output current. At the second stage, the pyroelectric potentials are gradually reduced and disappeared as the temperature variation vanished by retaining the power intensity of UV illumination, and the output current reaches a steady plateau labeled as $I_s$, where subscripts "s" indicate the steady output current. At the third stage, UV illumination is turned off and a sharp dip in output current (labeled as $I'_t$) induced by reverse pyro-potential distributions is observed due to instantaneous temperature decrease. At the fourth stage, the temperature returns to room temperature and stays stable with the pyro-potential slowly vanishing again due to leakage and screening, and thus the output current returns to a stable plateau (dark current) labeled as $I'_s$.

Typical four-stage current responses to various illumination light intensity are summarized and plotted in Figure 2b regarding to the absolute output currents $I_t$, $I_s$, and the relative peak-to-peak output currents $I_{tt'} = I_t - I'_t$. These results indicate that the currents monotonically increase with the power density of illumination and both absolute and relative currents can be utilized to evaluate the photosensing performances of pyro-phototronic effect based PDs. Besides, it is clear that the transient current $I_t$ is always larger than the conventional stable current $I_s$ with a maximal enhancement factor of 6.0 at the power density of $2.0 \times 10^{-4}$ W cm$^{-2}$ as shown in Figure S3 of the Supporting Information, while the peak-to-peak current $I_{tt'}$ is up to 869% larger than $I_s$ under $2.0 \times 10^{-4}$ W cm$^{-2}$ illumination.

To better understand the photosensing performance of the pyro-phototronic effect based PDs, the corresponding photoresponsivity $R$ is calculated and presented in Figure 2c based on $R = \frac{I_{light} - I'_s}{P_{ill}} = \frac{\eta_{ext} q}{h\nu} \cdot \gamma_G$,[29] where $P_{ill} = I_{ill} \times S$ is the illumination power on PDs, $I_{light}$ represent the absolute and/or relative output current under illumination, $\gamma_G$ is the internal gain, $\eta_{ext}$ is the external quantum efficiency (EQE), $q$ is electronic charge; $h$ is Planck's constant, $\nu$ is the frequency of the light, $I_{ill}$ is the excitation power density, and $S$ is the effective area of the PDs. For conventional stable output current $I_s$, the maximum of $R$ is derived as 2.17 mA $W^{-1}$ under illumination with a power density of $5.0 \times 10^{-5}$ W $cm^{-2}$. While the largest $R$ values reach 13 mA $W^{-1}$ with respect to the relative peak-to-peak transient currents, and 8.32 mA $W^{-1}$ for the absolute transient currents both at the power density of $3.0 \times 10^{-5}$ W $cm^{-2}$, indicating the enhancement factor of 599% and 383% by the pyro-phototronic effect, respectively. The achieved photoresponsivity is larger than that of the ZnO/CuSCN UV PDs (≈7.5 mA $W^{-1}$) and in the same order as that obtained from a Si/ZnO core-shell NW array PD ($1.0 \times 10^{-2}$ A $W^{-1}$, 480 nm, −1.0 V).[30,31] The corresponding specific detectivity $D^*$ is calculated as $D^* = R/(2q \cdot I'_s/S)^{0.5}$ to describe the smallest detectable signal by considering the dark current as the major noise (Figure S4, Supporting Information).[32] $D^*$ derived from the relative/absolute transient currents enhanced by the pyro-phototronic effect (labeled as $D^*_{tt}$ and $D^*_t$) display larger values than that derived from conventional stable currents related to the pure photoexcitation process (labeled as $D^*_s$).

Impacts of bias voltages on the pyro-phototronic effect are carefully studied by comparing the performances of devices operating under different bias voltages when applying a power density of $3.7 \times 10^{-3}$ W $cm^{-2}$ illumination as shown in **Figure 3**. $I$–$t$ characteristic of the PDs reversely biased at voltages ranging from 0.004 to 3.0 V is presented in Figure 3a. At reverse bias voltage smaller than 0.4 V, the output current demonstrates obvious four-stage responses in each cycle, clearly showing the pyro-phototronic effect in ZnO NWs. As the reverse bias voltage increasing, the dark-state current increase and the transient currents $I_t$ and $I'_t$ gradually disappear due to the compensation of pyro-phototronic effect by joule heating. These results indicate that the pyro-phototronic effect is controllable and highly dependent on bias voltage. Furthermore, the differences between transient and stable currents in both forward and reverse directions, ($I_t$– $I_s$) and ($I'_t$– $I'_s$) are plotted as a function of bias voltages as shown in Figure 3b. A local extreme value is observed at a reverse bias voltage of 0.4 V when turning on the UV light because as increasing the bias voltage, pyroelectric

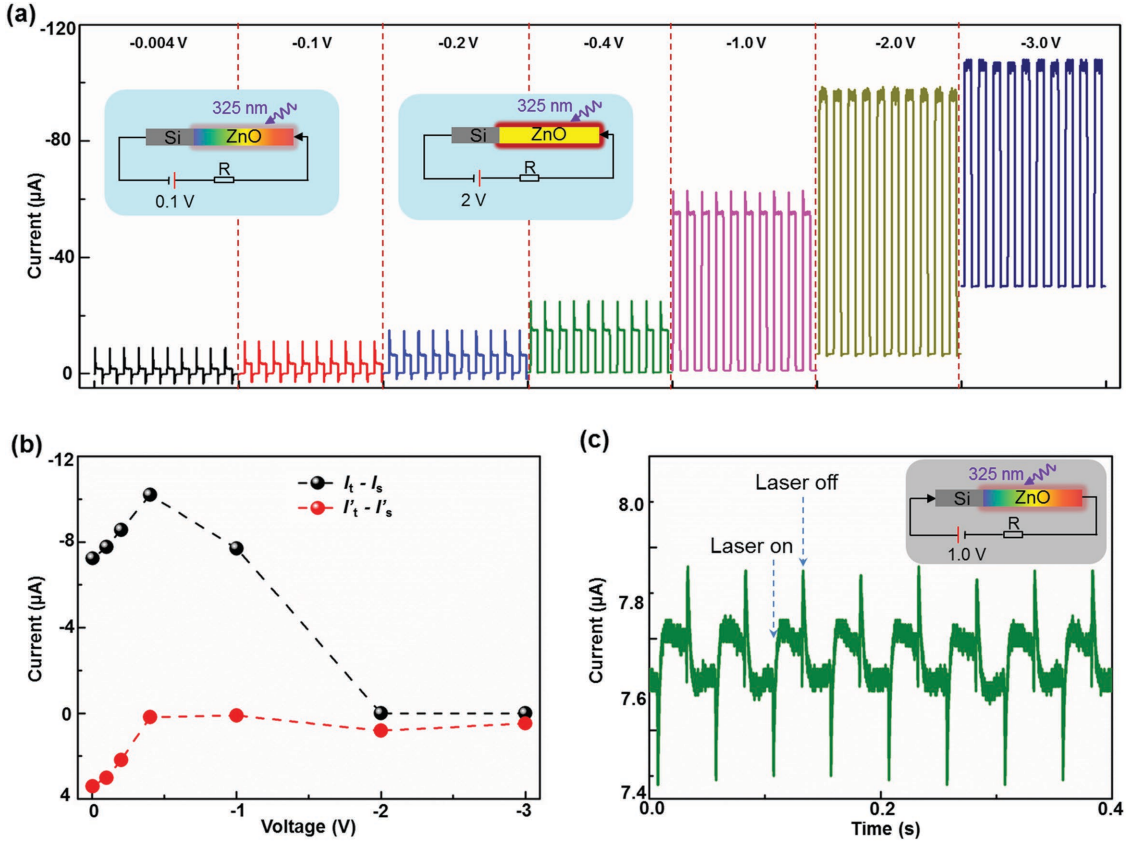


**Figure 3.** Impact of bias voltage on the pyro-phototronic effect. a) $I$–$t$ characteristics of the pyro-phototronic effect based PDs at different reverse bias voltages from 0.004 to 3.0 V (power density: $3.7 \times 10^{-3}$ W $cm^{-2}$). b) Differences between transient and stable currents in forward (black) and reverse (red) directions as a function of bias voltages. Data were extracted from $I$–$t$ curves in (a). c) $I$–$t$ curves of the pyro-phototronic effect based PDs at forward bias voltage of 1.0 V. The insets in (a) and (c) indicate the corresponding circuit diagram with current heating effect (red glow around ZnO) and pyroelectric potential in ZnO (color code in ZnO).



*Adv. Mater.* **2016**,
DOI: 10.1002/adma.201600884

polarizations decrease and photoconductivity increases within ZnO NWs to compete against each other. When turning off the UV light, the reverse peak disappears sooner than the forward peak with the increase of reverse bias voltage due to the monotonous decrease of reverse pyroelectric polarizations without any competing mechanism.

Further control experiments are conducted to demonstrate the UV sensing performances of the pyro-phototronic effect based PDs at forward biased voltages. As shown in Figure S5 of the Supporting Information, similar *I–t* characteristics to those derived at reversely biased voltages (Figure 2a) are observed, showing four-stages current–time responses at forward biased voltage of 0.004 V under the power density ranging from $3.7 \times 10^{-3}$ to $4.0 \times 10^{-6}$ W cm$^{-2}$. At forward biased voltage of 1.0 V, a combination of pyro-phototronic effect and photoexcitations in opposite directions are observed from the *I–t* curves shown in Figure 3c. Since the pyroelectric polarizations and the bias voltages are opposing each other at forward biased voltage (inset of Figure 3c), phenomenon of transient currents opposite to the direction of the stable currents are observed at the moment of turning on/off the light illumination. These results further confirm the working mechanism of light-self-induced pyro-phototronic PDs and provide guidance to designing such photodetectors by aligning the directions of pyro-polarizations and bias voltages to enhance the photosensing performances.

Pyro-phototronic effect enhancements on response time of the p-Si/n-ZnO PDs are carefully studied by comparing the performances of devices operating under $3.7 \times 10^{-3}$ W cm$^{-2}$ power density at the reverse bias voltage of 0.04 and 2.0 V as shown in **Figure 4**a,b. The rising time is defined as the time from 10% to 90% of maximum photocurrent and recovery time is defined as falling time from 90% to 10% of maximum photocurrent.[30,32] From Figure 4b, the response time of PDs with pyro-phototronic effect enhancements (–0.04 V bias voltage) at rising and falling edge are 19 and 22 µs, respectively. Compared to the response time of PD without pyro-phototronic enhancements (–2.0 V bias voltage) at rising/falling edge (59/40 µs), improvements of 311% in rising time and 182% in falling time are achieved by the light-self-induced pyro-phototronic effect in ZnO NWs. Considering the fact that the light illumination is controlled by an optical chopper operating at 1000 Hz, the actual response time of these PDs could be even faster. Moreover, the response time of p-Si/n-ZnO PDs under various illumination intensities are calculated and presented in Figure S6 of the Supporting Information. Different from tradition UV PDs that response fast under weak illuminations while slowly to strong light,[32] both the rising and falling time of these PDs decrease as increasing the power density, indicating a potential opportunity to fabricate fast response PD for strong light detections by utilizing the pyro-phtotronic effect.

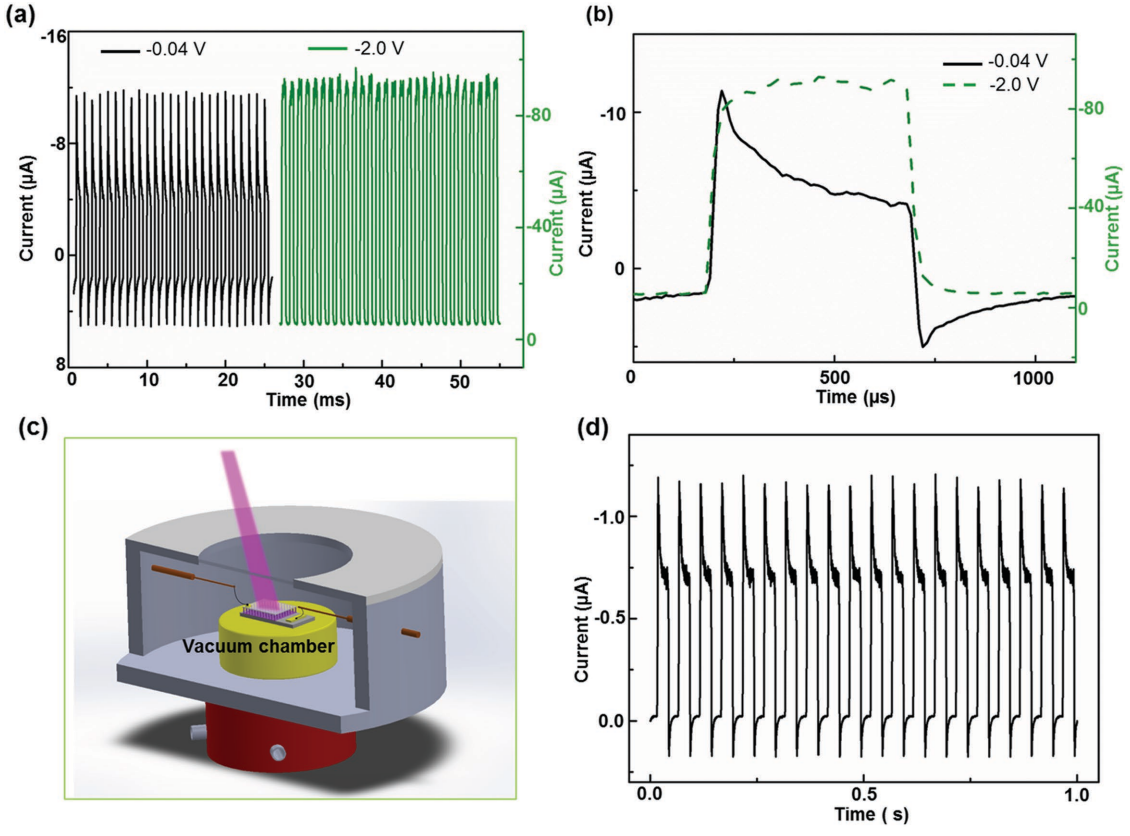


**Figure 4.** Response time of the pyro-phototronic effect based UV sensors. a) *I–t* characteristics of the pyro-phototronics PDs under the bias of –0.04 V (in black) and –2.0 V (in olive) and 325 nm laser illuminations through an optical chopper with a time ratio of 1:1 at 1000 Hz. b) Enlarged plot of a single output cycle as shown in (a) to demonstrate the role of the pyro-phototronic effect and calculate the response time. c) Schematic illustration of the experimental set-up of high vacuum chamber. d) *I–t* characteristics of the pyro-phototronic effect based PDs in vacuum ($2 \times 10^{-8}$ bar) by choosing the bias voltage of –0.04 V and the power density of $3.7 \times 10^{-3}$ W cm$^{-2}$, showing obvious four-stage current response to UV light.

Photosensing performances of the pyro-phototronic effect based PDs in vacuum condition is investigated and presented in Figure 4d by choosing the bias voltage of –0.04 V and the power density of $3.7 \times 10^{-3}$ W cm$^{-2}$. The vacuum chamber of a cryogenic probe system (Janis, model ST-500-2) as shown in Figure 4c is utilized to provide the vacuum condition ($2 \times 10^{-8}$ bar). Obviously, the typical four-stage current responses to UV illumination are observed in vacuum condition as shown in Figure 4d. The corresponding photoresponsivity $R$ is calculated to be 9.3 mA W$^{-1}$ with respect to the relative peak-to-peak transient currents, and 8.1 mA W$^{-1}$ for the absolute transient currents, comparable to the best results derived in air condition (13 and 8.32 mA W$^{-1}$, respectively). Furthermore, the response time at rising and falling edges are 1.5 and 1.2 ms even without correcting the electronic response of the measurement system, respectively, similar to that derived in air condition (Figure S6, Supporting Information) and smaller that of the reported UV PDs operating in air.[14,33] The result indicates the ultrafast photoresponse of pyro-phototronic PDs in vacuum condition, which is distinguished from the previous reported ZnO UV PDs that manifest weak and ultraslow photoresponse in vacuum.[6,17]

Visible light sensing performances of p-Si/n-ZnO photodetectors enhanced by the pyro-phototronic effect are studied and summarized in Figure S7 of the Supporting Information. $I$–$t$ characteristics of the PDs under 442 nm light illumination (1000 Hz) are presented in Figure S7 of the Supporting Information when the device is reversely biased at 0.4 V (Figure S7a, Supporting Information) and 4.0 V (Figure S7b, Supporting Information), respectively. It is clear that the output currents demonstrate different response behaviors under different bias voltages. The response time is improved from 20 μs (4.0 V) to 15 μs (0.4 V) at the rising edge and from 18 μs (4.0 V) to 12 μs (0.4 V) at the falling edge, corresponding to improvements of 33% and 50% of the rising and falling time due to the light-self-induced pyro-phototronic effect in ZnO NWs. The corresponding photoresponsivity derived from the relative transient currents is about 62 mA W$^{-1}$. The observed pyro-phototronic effect under 442 nm illuminations is resulted from the pyro-polarizations at the ZnO side as induced by the rapid temperature increase at the interface of p-Si/n-ZnO heterojunction due to the absorption of photons by both Si and ZnO.

To conclude, the light-self-induced pyro-photoronic effect, a three-way coupling effect among pyroelectric polarization, semiconductor properties, and optical excitation, has been utilized as an effective approach to achieve ultrafast response ultraviolet sensing in p-Si/n-ZnO heterostructures. As a result, the response time is improved from 59 to 19 μs at the rising edge, and 40 to 22 μs at the falling edge. Also, the response time of these PDs decrease as increasing the illumination power intensity, providing a potential opportunity for ultrafast detection of strong light. Besides, the responsivity is enhanced by up to 599% regarding to the relative changes of transient currents. Similar photosensing performances are achieved in both air and vacuum conditions. This newly designed ultrafast ultraviolet nanosensor is compatible to Si-based electronics/optoelectronics and thus may find promising applications in ultrafast photosensing, optothermal detections, health monitoring, and other optoelectronic processes.

## Experimental Section

*Fabrication Process of the p-Si/n-ZnO PDs*: P-type Si wafer was purchased from UniversityWafer Inc. (100 mm B-doped (100) wafer, 1–10 Ω cm, 500 μm SSP prime). ZnO seed layer was deposited by RF magnetron sputtering (PVD75, Kurt. J. Lesker Company) at the power of 120 W and chamber pressure of 8 mTorr for 30 min, with the thickness of 100 nm. The coated p-Si are then placed into the mixed nutrient solutions (0.02 M $Zn(NO_3)_2$ and 0.02 M hexamethylenetetramine) for ZnO NWs growth via a hydrothermal method in a mechanical convection oven (model Yamato DKN400, Santa Clara, CA, USA) at 85 °C for 30 min. In order to get separated ZnO NWs, 0–5 mL ammonium hydroxide (Sigma-Aldrich) is added per 100 mL mixing solution. After cooling down the whole system, the product is washed by ethanol and distilled water, collected and vacuum-dried at 100 °C for 1 h. Then a thin layer of ITO is deposited on ZnO as the top electrode and Cu is sputtered on p-Si as bottom electrode. Testing wires are connected to top and bottom electrodes by silver paste. Finally, a thin layer of kapton tape is applied to fix the testing wires and improve its robustness.

*Materials Characterizations*: Detailed microscopic structures of ZnO NWs are characterized by scanning electron microscope (SEM) (Hitachi SU8010).

*Optical and Electrical Measurements*: Transmission spectra of ZnO are measured by an UV–vis spectrophotometer (JASCO V-630). $I$–$V$ characteristics of the device are measured and recorded by a customized computer-controlled measurement system with Stanford SRS Low noise current preamplifier (SR570)/SRS Low noise voltage preamplifier (SR560) in conjunction with a GPIB controller (GPIB-USB-HS, NI 488.2). The optical input stimuli are provided by a He-Cd dual-color laser (Model No. IK5751I-G, Kimmon Koha Co., Ltd.). A continuously variable filter was used to control the light power density. The corresponding power density is measured by a thermopile powermeter (Newport 818P-001-12). An UV objective is used to expand 325 nm laser to illuminate the whole device in air. And the effective size of the device is 10 mm × 10 mm. The vacuum condition ($2 \times 10^{-8}$ bar) is provided by the vacuum chamber of a micromanipulation cryogenic probe system (Janis, model ST-500-2). UV objective is not used for beam expansion in vacuum condition.

## Supporting Information

Supporting Information is available from the Wiley Online Library or from the author.

## Acknowledgements

Z.W. and R.Y. contributed equally to this work. This research was supported by the Research was supported by U.S. Department of Energy, Office of Basic Energy Sciences (Award No. DE-FG02-07ER46394), the National Science Foundation (DMR-1505319), National Natural Science Foundation of China (Grant Nos. 51432005, 11574033, and 11104016), the "thousands talents" program for pioneer researcher and his innovation team, Beijing Higher Education Young Elite Teacher Project and the Fundamental Research Funds for the Central Universities (No. 2015KJJCB02).

Received: February 14, 2016
Revised: May 5, 2016
Published online:

[1] E. Monroy, F. Omnes, F. Calle, *Semicond. Sci. Technol.* **2003**, *18*, R33.
[2] R. M. Yu, C. F. Pan, Z. L. Wang, *Energy Environ. Sci.* **2013**, *6*, 494.

[3] R. M. Yu, C. F. Pan, J. Chen, G. Zhu, Z. L. Wang, *Adv. Funct. Mater.* **2013**, *23*, 5868.
[4] C. F. Pan, L. Dong, G. Zhu, S. M. Niu, R. M. Yu, Q. Yang, Y. Liu, Z. L. Wang, *Nat. Photonics* **2013**, *7*, 752.
[5] D. C. Kim, B. O. Jung, Y. H. Kwon, H. K. Cho, *J. Electrochem. Soc.* **2012**, *159*, K10.
[6] C. Soci, A. Zhang, B. Xiang, S. A. Dayeh, D. P. R. Aplin, J. Park, X. Y. Bao, Y. H. Lo, D. Wang, *Nano Lett.* **2007**, *7*, 1003.
[7] H. Kind, H. Q. Yan, B. Messer, M. Law, P. D. Yang, *Adv. Mater.* **2002**, *14*, 158.
[8] Z. Wang, R. Yu, X. Wen, Y. Liu, C. Pan, W. Wu, A. Z. L. Wang, *ACS Nano* **2014**, *8*, 12866.
[9] Q. Yang, X. Guo, W. H. Wang, Y. Zhang, S. Xu, D. H. Lien, Z. L. Wang, *ACS Nano* **2010**, *4*, 6285.
[10] S. E. Ahn, J. S. Lee, H. Kim, S. Kim, B. H. Kang, K. H. Kim, G. T. Kim, *Appl. Phys. Lett.* **2004**, *84*, 5022.
[11] K. Keem, H. Kim, G. T. Kim, J. S. Lee, B. Min, K. Cho, M. Y. Sung, S. Kim, *Appl. Phys. Lett.* **2004**, *84*, 4376.
[12] M. C. Jeong, B. Y. Oh, W. Lee, J. M. Myoung, *Appl. Phys. Lett.* **2005**, *86*, 103105.
[13] Y. F. Hu, J. Zhou, P. H. Yeh, Z. Li, T. Y. Wei, Z. L. Wang, *Adv. Mater.* **2010**, *22*, 3327.
[14] G. Cheng, X. H. Wu, B. Liu, B. Li, X. T. Zhang, Z. L. Du, *Appl. Phys. Lett.* **2011**, *99*, 203105.
[15] Z. Wang, R. Yu, C. Pan, Y. Liu, Y. Ding, a. Z. Wang, *Adv. Mater.* **2015**, *27*, 1553.
[16] S. Bai, W. W. Wu, Y. Qin, N. Y. Cui, D. J. Bayerl, X. D. Wang, *Adv. Funct. Mater.* **2011**, *21*, 4464.
[17] Q. H. Li, T. Gao, Y. G. Wang, T. H. Wang, *Appl. Phys. Lett.* **2005**, *86*, 123117.
[18] M. Razeghi, A. Rogalski, *J. Appl. Phys.* **1996**, *79*, 7433.
[19] C. C. Hsiao, S. Y. Yu, *Sensors-Basel* **2012**, *12*, 17007.
[20] Y. Yang, W. X. Guo, K. C. Pradel, G. Zhu, Y. S. Zhou, Y. Zhang, Y. F. Hu, L. Lin, Z. L. Wang, *Nano Lett.* **2012**, *12*, 2833.
[21] C. C. Hsiao, S. W. Huang, R. C. Chang, *Sensor Mater.* **2012**, *24*, 421.
[22] Z. Wang, R. Yu, C. Pan, Z. Li, J. Yang, F. Yi, Z. L. Wang, *Nat. Commun.* **2015**, *6*, 8401.
[23] Y. Liu, A. Das, S. Xu, Z. Y. Lin, C. Xu, Z. L. Wang, A. Rohatgi, C. P. Wong, *Adv. Energy Mater.* **2012**, *2*, 47.
[24] Y. Xie, M. Madel, Y. J. Li, W. Q. Jie, B. Neuschl, M. Feneberg, K. Thonke, *J. Appl. Phys.* **2012**, *112*, 123111.
[25] S. M. Sze, *CC/Eng. Technol. Appl. Sci.* **1982**, *27*, 28.
[26] J. A. Aranovich, D. Golmayo, A. L. Fahrenbruch, R. H. Bube, *J. Appl. Phys.* **1980**, *51*, 4260.
[27] S. Mridha, D. Basak, *J. Appl. Phys.* **2007**, *101*, 083102.
[28] Y. Liu, S. M. Niu, Q. Yang, B. D. B. Klein, Y. S. Zhou, Z. L. Wang, *Adv. Mater.* **2014**, *26*, 7209.
[29] G. Konstantatos, E. H. Sargent, *Nat. Nanotechnol.* **2010**, *5*, 391.
[30] S. M. Hatch, J. Briscoe, S. Dunn, *Adv. Mater.* **2013**, *25*, 867.
[31] K. Sun, Y. Jing, N. Park, C. Li, Y. Bando, D. L. Wang, *J. Am. Chem. Soc.* **2010**, *132*, 15465.
[32] X. Liu, L. L. Gu, Q. P. Zhang, J. Y. Wu, Y. Z. Long, Z. Y. Fan, *Nat. Commun.* **2014**, *5*, 4007.
[33] J. Zhou, Y. D. Gu, Y. F. Hu, W. J. Mai, P. H. Yeh, G. Bao, A. K. Sood, D. L. Polla, Z. L. Wang, *Appl. Phys. Lett.* **2009**, *94*, 191103.